THE JOURNAL OF BIOLOGICAL CHEMISTRY VOL. 282, NO. 42, pp. 30658–30666, October 19, 2007

Mutations Designed to Destabilize the Receptor-Bound Conformation Increase MICA-NKG2D Association Rate and Affinity*

Received for publication, June 1, 2007, and in revised form, July 30, 2007 Published, JBC Papers in Press, August 8, 2007, DOI 10.1074/jbc.M704513200

Candice S. E. Lengyel[‡], Lindsey J. Willis[‡], Patrick Mann[‡], David Baker[§], Tanja Kortemme[¶], Roland K. Strong[‖], and Benjamin J. McFarland[‡1]

From the [‡]Department of Chemistry and Biochemistry, Seattle Pacific University, Seattle, Washington 98119, the [§]Department of Biochemistry, University of Washington, Seattle, Washington 98195, the [¶]Department of Biopharmaceutical Sciences, University of California, San Francisco, California 94143, and the [‖]Division of Basic Sciences, Fred Hutchinson Cancer Research Center, Seattle, Washington 98109

MICA is a major histocompatibility complex-like protein that undergoes a structural transition from disorder to order upon binding its immunoreceptor, NKG2D. We redesigned the disordered region of MICA with RosettaDesign to increase NKG2D binding. Mutations that stabilize this region were expected to increase association kinetics without changing dissociation kinetics, increase affinity of interaction, and reduce entropy loss upon binding. MICA mutants were stable in solution, and they were amenable to surface plasmon resonance evaluation of NKG2D binding kinetics and thermodynamics. Several MICA mutants bound NKG2D with enhanced affinity, kinetic changes were primarily observed during association, and thermodynamic changes in entropy were as expected. However, none of the 15 combinations of mutations predicted to stabilize the receptor-bound MICA conformation enhanced NKG2D affinity, whereas all 10 mutants predicted to be destabilized bound NKG2D with increased on-rates. Five of these had affinities enhanced by 0.9–1.8 kcal/mol over wild type by one to three non-contacting substitutions. Therefore, in this case, mutations designed to mildly destabilize a protein enhanced association and affinity.

NKG2D-ligand interactions play a central role in inducible NK cell and γδ T cell activation, initiating cytotoxic responses to transformation and infection (1–3). All known NKG2D-binding proteins use a major histocompatibility complex platform-like tertiary structure as a scaffold to contact NKG2D, including two binding surface α helices (α1 and α2). In the crystal structure of the NKG2D ligand MICA, electron density was absent for a central portion of the α2 helix (residues 152–161), indicating that the helix in that region was disordered into a flexible loop (4). When bound to NKG2D, the residues were ordered beneath the receptor (5). This type of transition from disorder to order upon binding is similar to other immunoreceptor-ligand combinations (6–9). The thermodynamics of four NKG2D-ligand interactions were compared and found to be driven by both enthalpy and entropy, distinct from the generally enthalpy-driven, entropy-hindered T-cell receptor-major histocompatibility complex interactions (10).

The structural characterization of NKG2D-ligand interfaces allows computational optimization of the interactions. Algorithms for computational design of proteins have already been used for energetic dissection of NKG2D-ligand interactions, confirmed by experiment (11). Different rational design techniques applied to LFA-1 with ICAM-1 (intercellular adhesion molecule 1) (12) and a mature antibody-antigen complex (13), for example, have engineered interfaces toward increased affinities.

We applied rational design to the MICA-NKG2D interface by attempting to stabilize MICA in its receptor-bound conformation. Loss of configurational freedom for the MICA α2 loop should pose an entropic barrier to MICA-NKG2D association, assuming protein entropy dominates. Using RosettaDesign, we used a two-stage design strategy to stabilize this region of MICA with the goal of reducing the entropic barrier to protein-protein association, altering MICA minimally to maintain global protein stability and retain most NKG2D contacts. We predicted that successful redesign would alter only the association rate, leaving dissociation kinetics unchanged, and would therefore increase affinity through a more favorable entropy of interaction. To test this, we created 25 mutant MICA molecules that were amenable to thermodynamic binding analysis. As expected, many mutants bound NKG2D significantly faster than wild-type but dissociated at a similar rate, and hence had increased affinity for NKG2D. Van't Hoff thermodynamics were also consistent with our hypothesis, but entropic stabilization was compensated with enthalpic destabilization. Surprisingly, the design scores for the tight-binding MICA mutants were *worse* than for wild type; for these mutants, RosettaDesign predicts mild destabilization of the receptor-bound MICA conformation.

EXPERIMENTAL PROCEDURES

Computational Protein Design—Computational protein design methods seek to identify low energy sequences compatible with a given protein structure or function. Here we aimed to stabilize MICA in its bound conformation, as observed in the

* The costs of publication of this article were defrayed in part by the payment of page charges. This article must therefore be hereby marked "*advertisement*" in accordance with 18 U.S.C. Section 1734 solely to indicate this fact.
[1] To whom correspondence should be addressed: 3307 3rd Ave. W, Suite 205, Seattle, WA 98119-1997. Tel.: 206-281-2749; Fax: 206-281-2882; E-mail: bjm@spu.edu.

MICA-NKG2D structure. We first identified eight sequence positions on MICA for redesign (see "Results"). At each of these positions we sampled rotameric conformations of 19 naturally occurring amino acids (except cysteine) during the design simulations. Sequences and side-chain conformations were optimized for the bound MICA backbone using Monte-Carlo simulated annealing and a scoring function dominated by Lennard-Jones atomic packing interactions, hydrogen bonding, and an implicit solvation model, as previously described (14). We collected 500 low energy sequences from the design simulations and used the most frequently observed amino acids at each position in this set to compile a computational library (Table 1). We also included the wild-type amino acid at each position, yielding a total of 4608 sequence combinations. We then built models for all sequence combinations in this library, where the MICA backbone was held fixed in the bound conformation observed in the MICA-NKG2D complex structure and the side-chain conformations of all designed residues were varied. All models were then ranked using the scoring function applied during design.

Protein Expression and Purification—Human NKG2D (residues 90–216) and MICA*001 (residues 1–274, plus a C-terminal 6-histidine tag) plasmids were altered with the QuikChange II site-directed mutagenesis kit (Stratagene), sequenced using capillary electrophoresis, and were overexpressed as inclusion bodies in BL21-DE3-RIL cells (Stratagene). (Bacterial expression can be used because glycosylation of MICA does not affect NKG2D interaction (5).) Cells were lysed mechanically using 1-mm glass beads (BeadBeater/BioSpec); 30-min incubations at room temperature with 10 mM dithiothreitol, 1 mg/ml lysozyme, and 1 mg/ml DNase; and multiple freeze/thaw cycles and washes with 0.5% Triton X-100. (All chemicals were purchased from Sigma except where noted.) Inclusion bodies were collected by centrifugation and dissolved in 8 M urea/100 mM Tris/50 mM glycine, pH 8.0, placed in Snakeskin 10-kDa dialysis tubing (Pierce), and dialyzed using overnight steps into 2-liter solutions of 4 M, 2 M, 1 M, and 0 M urea, also containing 100 mM Tris, pH 8.0/400 mM L-arginine/0.5 mM EDTA/0.02% sodium azide. Protein was then dialyzed overnight into standard Qiagen nitrilotriacetic acid binding buffer (for MICA) or 10 mM phosphate, pH 8.0 (for NKG2D). Standard procedures for nickel-nitrilotriacetic acid (Qiagen) or High-Q ion exchange (Bio-Rad) chromatography were used to purify MICA and NKG2D, respectively. The purity of each protein sample was confirmed to be >95% by SDS-PAGE. All proteins were purified by Superdex 200 size-exclusion chromatography (SEC)[2] within 72 h of use and showed no evidence of aggregation by additional analytical SEC within that time period with the exception of MICQ120I_K154M. After elution from the column, concentration was found by bicinchoninic acid (BCA) assay (Pierce), as confirmed by Nanodrop UV-visible analysis.

CD Analysis—Experiments were patterned after analysis of soluble major histocompatibility complex class I-peptide complexes (15) and redesigned small proteins (16). 5–20 μM solutions of MICA proteins were dialyzed into 25 mM potassium phosphate, pH 7.0. The ellipticity at 220 nm was measured with an Aviv 62A DS spectrometer from 20 to 98 °C with 1° steps (2-mm pathlength). Wild-type and mutant melts were irreversible. The melting temperature (T_m) was determined by fitting the data to a Gibbs-Helmholtz equation and normalizing to the parameters from the fit (16). Three wild-type melts produced T_m values within 1 °C, as did multiple melts for mutants.

Fluorescence Quenching—Intrinsic tryptophan fluorescence was measured using a PerkinElmer Life Sciences LS 55 fluorometer and ~0.2 μM SEC-pure MICA samples in HBS-EA buffer (10 mM HEPES (pH 7.4), 150 mM NaCl, 3 mM EDTA, and 0.02% sodium azide) in a 10-mm quartz cuvette, 280 nm excitation and 300–500 nm or 350 nm emission, with both slit widths at 10.0 nm. The sample was titrated with a 3 M acrylamide solution. Scans were repeated three times and averaged. Fluorescence readings of a blank HBS-EA sample were subtracted, and the readings were corrected for titrant dilution (never exceeding 10%). Each sample was also corrected for inner filter effects as described previously (17).

Surface Plasmon Resonance Analysis—A BIAcore 3000 surface plasmon resonance (SPR) instrument was equilibrated in HBS-EP buffer (10 mM HEPES (pH 7.4), 150 mM NaCl, 3 mM EDTA, and 0.05% P-20, BIAcore AB). 0.05% P-20 was added to all protein samples. MICA proteins were coupled to research-grade CM5 chips using standard NHS-based amine-coupling chemistry (BIAcore AB). (NKG2D was inactive upon amine coupling, probably due to positively charged residues near the active site.) The first or third flow cells were subjected to the chemical steps of coupling to serve as an internal blank. Ligand coupling densities resulting in ~50 maximum response units upon NKG2D injection were used for wild-type and most mutants; the same conditions resulted in surfaces for high affinity mutants where R_{max} ~100–300 response units. Coupling of lower or higher ligand densities did not change the kinetic constants measured within error.

NKG2D was injected at 40 μl/min at 25 °C. Flow rates of 20–100 μl/min did not change NKG2D association or dissociation phases. For each experiment, 1–9 μM NKG2D samples serially diluted five to six times were injected, along with three buffer blanks. Each experiment was independently repeated three to five times with average buffer blank and flow cell blank-corrected values and standard errors reported. For equilibrium binding constants, the average responses from the last 5–15 s of NKG2D injection were fit to a steady-state binding model. For kinetic constants, the first 80 s of data collection after NKG2D injection within a set of 4–6 injections were globally fit to a standard 1:1 Langmuir binding model using BIAevaluation 3.0 software (BIAcore AB). For biphasic kinetics, the data show some slow (k_{+2}, $k_{-1} < 1\ s^{-1}$) kinetic complexity and were globally fit to a standard two-step reaction (conformation change model) using BIAevaluation 3.0 software. Reaction 1 shows the simplest way to model a biphasic protein-protein interaction,

$$A + B \underset{k_{-1}}{\overset{k_{+1}}{\rightleftharpoons}} [AB]^* \underset{k_{-2}}{\overset{k_{+2}}{\rightleftharpoons}} AB$$

REACTION 1

[2] The abbreviations used are: SEC, size-exclusion chromatography; SPR, surface plasmon resonance; ITC, isothermal titration calorimetry.

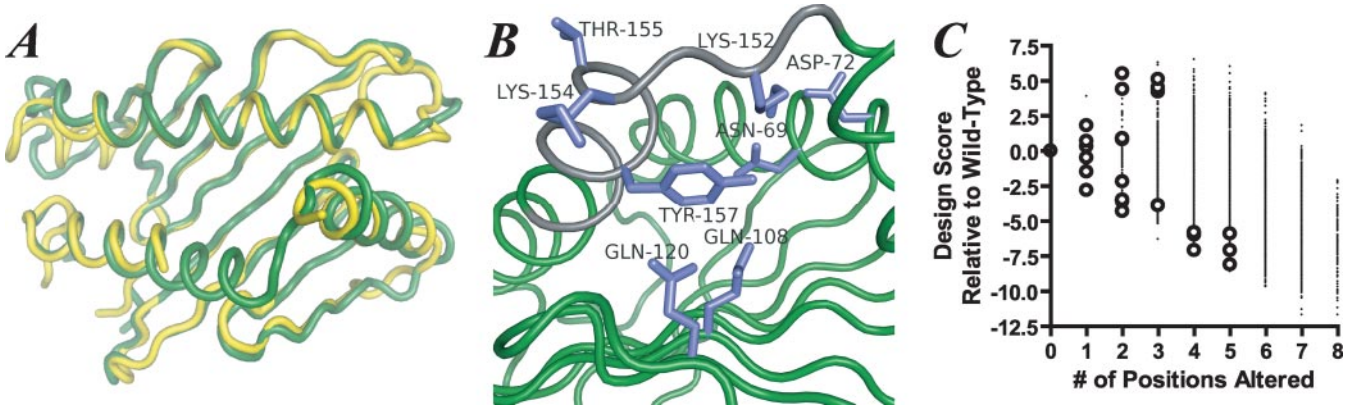

FIGURE 1. **Design locations and strategy.** *A*, the crystal structure of unbound MICA (*yellow*, PDB ID: 1B3J) superimposed on the crystal structure of the MICA/NKG2D complex (*green*, PDB ID: 1HYR). *B*, side view of receptor-bound MICA structure used for design with eight design target residues shown as sticks and labeled. *C*, design space explored in the second round of RosettaDesign. Designs are represented as RosettaDesign-predicted scores relative to wild type (arbitrary units, more negative indicates predicted stabilization of MICA in its bound conformation) *versus* number of residues altered from wild-type MICA. Designs are indicated as follows: wild type and designs expressed, refolded, and assayed in this study (○); designs scored in the second round but not experimentally investigated (■). *A* and *B* were generated with PyMOL (W. L. DeLano (2002) PyMOL, DeLano Scientific, San Carlos, CA).

TABLE 1

Locations of designed residues in MICA and comparison to known allelic polymorphism

MICB or other = residues appearing in other alleles of MICA or in MICB alleles as summarized previously (8). First round = residues selected from the first round of RosettaDesign analysis in addition to wild type. Best and worst 20 = residues appearing at each position more than once in the 20 designs with lowest design scores ("best") and those with highest design scores ("worst").

MICA residue	Wild type	MICB or other	First round	Best 20	Worst 20
69	Asn	Asn	Leu, Gln, Trp	Gln	Trp
72	Asp	Asp	Phe, Trp	Phe, Asp	Trp
108	Gln	Arg	Leu, Arg	Arg	Gln
120	Gln	Gln	Ile	Ile	Gln, Ile
152	Lys	Lys	Glu, Phe, Val	Val	Glu
154	Lys	Lys	Asp, Met, Ser	Ser	Met
155	Thr	Thr	Asp	Asp	Thr
157	Tyr	Tyr, Leu, Arg	Leu	Leu	Tyr

where A and B are the MICA variant and NKG2D, $[AB]^*$ is an intermediate encounter complex, and AB is the final, fully engaged protein complex. Reaction 1 is written in induced fit form, although the conformational change may either precede binding (pre-equilibrium) or coincide with binding (induced fit).

As previously observed, wild-type MICA at high NKG2D concentrations shows some kinetic complexity too fast for SPR to detect (10), which also appears for mutant MICA with mutations predicted to stabilize the receptor-bound conformation (see Fig. 3*D*). These were fit as refractive index offsets within the Langmuir model, because no kinetic information could be derived. If the offset is removed, a poorer fit results, the change in $\Delta\Delta G$ is <10%, and the rank order of mutations is not changed, but increases relative standard errors, and the residuals of the equation fits increase systematically. At equilibrium, all kinetic phases contribute, and $\Delta\Delta G_{eq}$ correlates with $\Delta\Delta G_{kin\ obs}$ (see Fig. 3*G*).

Several control experiments were used to confirm that none of the multiple kinetic phases observed in these sensorgrams could be caused by transiently formed aggregates or other impurities: 1) MICA mutants were specifically oriented on a chip by binding to an amine-coupled antibody specific for the α3 domain; 2) a lower ligand density of the MICA mutant was used (both amine-coupled and antibody-oriented); and 3) we injected samples of NKG2D that were not size-purified or were size-purified months before, containing more multimeric,

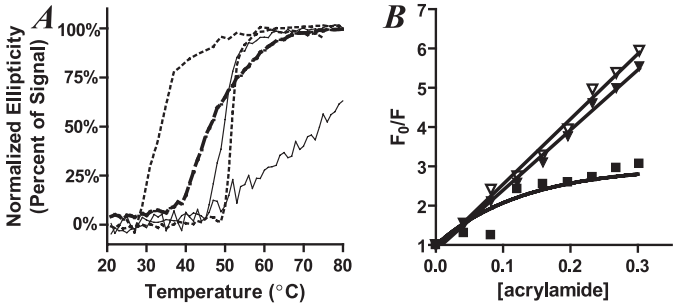

FIGURE 2. **Characterization of MICA mutants in solution.** *A*, normalized CD signal at 220 nm *versus* temperature. Lines and T_m values are as follows: *Dashed line* = MICA wild type, 47.5 °C; *dotted lines* = predicted-destabilized mutants with highest and lowest T_m values, MICN69W_K152E, 51.9 °C and MICK152E_K154M, 33.0 °C; *solid lines* = predicted-stabilized mutants with highest and lowest T_m values, MICN69Q_Q108L_Q120I_K154S_T155D, >75 °C and MICN69Q, 50.0 °C. Predicted-stabilized mutants not shown = MICK154D, 52.5 °C; MICN69Q_K154D, 52.6 °C; and MICN69Q_D72F_Q108L_K152V_Y157L, 54.6 °C. Predicted-destabilized mutants not shown = MICN69W_K152E_K154D, 51.8 °C; MICN69W_D72F_K152E, 51.6 °C; and MICQ120I, 40.2 °C. (*B*) Stern-Volmer plot of quenched fluorescence *versus* concentration of titrated acrylamide. Quenched fluorescence is F_0/F, where F_0 is original fluorescence at 350 nm and F is corrected acrylamide-quenched fluorescence at 350 nm. Wild-type MICA (■); MICN69W_K154E (▽); and MICN69W_D72W_K154E (▼).

aggregated forms of the receptor. In all cases, multiphasic kinetics were obtained that were identical within error to those obtained from the typical amine-coupled MICA mutant chip, showing that the fast on/off phases are not caused by weak, nonspecific association of aggregate. Therefore, the complex kinetics are not caused by nonspecific binding of trace amounts

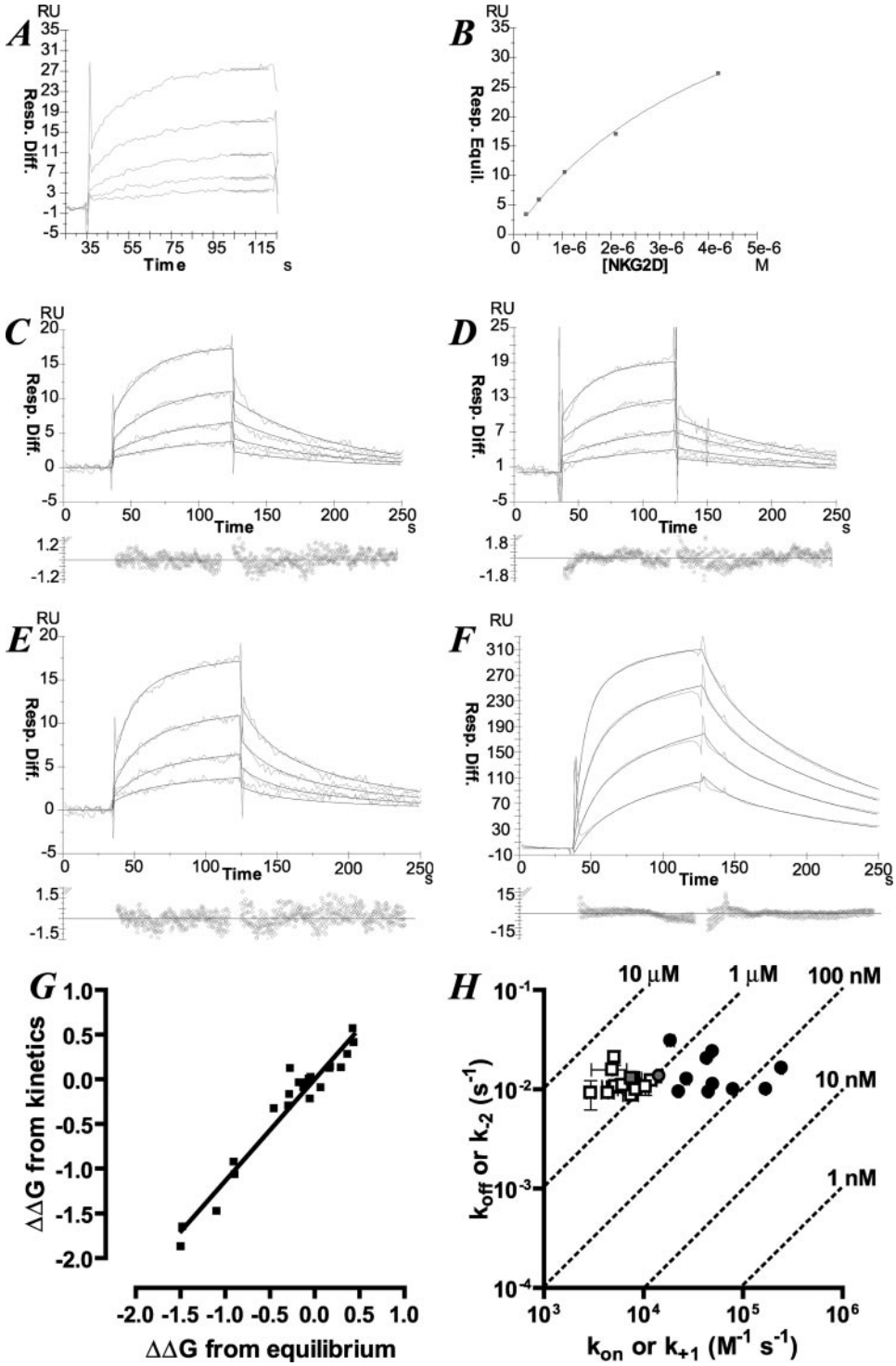

FIGURE 3. **Surface plasmon resonance equilibrium and kinetic analysis of MICA-NKG2D interactions.** *A*, representative wild-type MICA/NKG2D interaction showing the approach to observed equilibrium after 90 s of analyte injection, with serially diluted concentrations as recorded in the *x*-axis of *B*. *B*, equilibrium response *versus* [NKG2D] plot used to determine wild-type equilibrium affinity. *C*, representative sensorgrams of wild type and *D*, MICN69Q_Q120I _K154S_T155D_Y157L, showing association and dissociation phases as well as global kinetics fits to a 1:1 Langmuir binding model with residuals below, [NKG2D] in serial dilutions similar to *A*. All data were referenced to an inline blank CM5 surface and to three blank buffer injections before each set of NKG2D injections. *E*, representative sensorgrams of wild type and *F*, MICN69W_K152E, showing data fit to a two-state (conformational change) model from BIAevaluation 3.0 with fit residuals below. *G*, $\Delta\Delta G$ ($= \Delta G$ mutant $- \Delta G$ wild type) determined by kinetic *versus* equilibrium methods from SPR data, in kcal mol^{-1} units. The fit line has a slope of 1.1 $\pm$ 0.1, a *y*-intercept of 0.00 $\pm$ 0.04 and $R^2 = 0.944$. *H*, $k_{off\,obs}$ *versus* $k_{on\,obs}$, or for biphasic fits k_{-2} *versus* k_{+1}, for NKG2D interacting with MICA mutants. The *dotted lines* represent different K_D values, as labeled. MICA mutants are labeled as follows: monophasic mutants with predicted stabilization of the receptor-bound conformation (□), with wild type in *gray*; and biphasic mutants with predicted destabilization of the wild-type conformation (●), with wild type in *gray*.

of multimeric forms of MICA (control #2) or NKG2D (control #3), or by heterogeneity in the amine coupling process (controls #1 and 2). In addition, sample homogeneity was assured, because proteins were prepared from inclusion bodies, no other proteins or forms of protein were detectable by SDS-PAGE or SEC, and all experimental samples were SEC-purified before use in quantitative SPR assays. Finally, k_{+2} was concentration-independent at high concentrations (see Fig. 3*F*), whereas weak, nonspecific binding would be concentration-dependent, increasing significantly at high receptor concentrations (18).

Size-exclusion Binding Assay—10–20 μg of NKG2D and MICA proteins in the 1–5 μM range, either alone or mixed in a 1:1 molar ratio, were injected onto a 10/300 GL Superdex 200 FPLC column (General Electric Healthcare) equilibrated in HBS-EA buffer, and peaks were detected by absorbance at 280 nm. Columns were calibrated with protein standards (GE Healthcare).

Isothermal Titration Calorimetry—A MicroCal VP-ITC instrument was used with 9.3 μM human NKG2D in 1.4 ml of HBS-EA in the calorimetric cell. All solutions were size-exclusion-purified, concentrated, and degassed immediately before use. Aliquots (8 μl) of 110 μM MICN69W_K152E in HBS-EA were added stepwise to the stirred NKG2D solution with 240-s spacing. The heat evolved was calculated by fitting the data with Origin software.

RESULTS

Two-stage Design of MICA Helix-Loop Stabilization—Disorder at the MICA-NKG2D binding interface was targeted for stabilization. Electron density corresponding to the α2 helix residues 152–161 does not appear in the crystal structure of MICA alone, but when NKG2D is bound, those residues are folded into two turns of a helix and a short loop (Fig. 1*A*). We designed mutations to stabilize the receptor-bound conformation of the α2

TABLE 2

MICA mutants predicted to stabilize the receptor-bound conformation and fit with a monophasic kinetic model

All thermodynamic values are given at 25 °C in kcal mol^{-1}. Des. Score Rel. to WT = mutant design score – wild-type design score; design scores are computed for the MICA monomer in its bound conformation, with lower numbers meaning that the stability is predicted to be increased. N/A = kinetic data could not be measured due to weak overall affinity.

MIC mutant	Des. score rel. to WT	ΔG_{eq}	$k_{on,\ obs}/10^3$	$k_{off,\ obs}/10^{-3}$	$\Delta G_{kin\ obs}$	ΔH_{VH}
			$M^{-1}\,s^{-1}$	s^{-1}		
N69Q_Q108L_Q120I_K154S_T155D	−8.1	−7.3 ± 0.1	7.5 ± 1.3	8.7 ± 0.4	−8.1 ± 0.1	−1.3 ± 2.5
N69Q_Q120I_K154S_T155D_Y157L	−7.1	−7.0 ± 0.2	5.0 ± 1.1	10.4 ± 0.7	−7.7 ± 0.2	−1.3 ± 1.9
N69Q_D72F_K154S_T155D	−7.1	−7.2 ± 0.3	N/A	N/A	N/A	N/A
N69Q_Q120I_K154S_T155D	−6	−7.2 ± 0.1	5.2 ± 1.4	10.7 ± 0.3	−7.7 ± 0.2	−1.0 ± 1.7
N69Q_D72F_Q108L_K152V_Y157L	−5.9	−6.2 ± 0.1	5.1 ± 0.6	20.9 ± 3.5	−7.4 ± 0.1	1.1 ± 1.4
K152V_K154S_T155D_Y157L	−5.8	−7.0 ± 0.1	3.0 ± 0.3	9.2 ± 3.0	−7.6 ± 0.2	−2.7 ± 2.7
N69Q_K154D	−4.3	−7.6 ± 0.3	8.4 ± 2.9	9.9 ± 0.5	−8.0 ± 0.2	4.2 ± 2.1
K154S_T155D	−4	−7.7 ± 0.2	N/A	N/A	N/A	N/A
K152V_K154S_T155D	−3.9	−6.9 ± 0.2	4.9 ± 1.9	15.7 ± 1.4	−7.4 ± 0.3	−1.7 ± 1.6
N69Q_D72F_Q108L	−3.9	−7.4 ± 0.2	6.2 ± 1.1	11.0 ± 1.8	−7.8 ± 0.1	0.3 ± 1.5
N69Q_D72F	−3.6	−7.7 ± 0.2	4.4 ± 0.7	9.2 ± 1.0	−7.7 ± 0.1	1.3 ± 1.4
N69Q	−2.8	−7.4 ± 0.1	12.0 ± 1.6	12.3 ± 1.3	−8.2 ± 0.1	3.7 ± 1.0
K152V_Y157L	−2.2	−7.5 ± 0.1	8.0 ± 1.5	12.9 ± 1.2	−7.9 ± 0.1	0.6 ± 1.8
K154D	−1.5	−7.4 ± 0.1	7.8 ± 1.3	12.7 ± 1.8	−7.9 ± 0.2	3.9 ± 1.7
Q108L	−0.5	−7.8 ± 0.1	10.0 ± 1.0	10.6 ± 1.9	−8.2 ± 0.1	1.1 ± 1.9
Wild type	0	−7.3 ± 0.1	7.5 ± 1.1	13.0 ± 0.9	−7.8 ± 0.1	−3.5 ± 1.4

helix-loop by optimizing the α2 contacts with the rest of MICA in the receptor-bound conformation. Using the coordinates from the receptor-bound MICA structure as a design template, we selected residues as design targets in the region disordered in the unbound structure but away from the direct contact interface with NKG2D. This yielded four residues in the center of the α2 helix-loop, and four residues that interact with α2 residues: two from the α1 helix and two from the β sheet underneath (Fig. 1*B*). Only residue Thr-155 was observed contacting NKG2D in the crystal structure (5).

We optimized MICA using a two-stage strategy: we first allowed non-cysteine amino acid residue substitutions at all selected positions simultaneously during RosettaDesign runs (see Methods), and we selected sequences predicted to stabilize MICA relative to wild-type in the backbone conformation found in the NKG2D-bound MICA structure. Simulations were performed using a Monte-Carlo simulated annealing procedure, and sequences were ranked by a scoring function dominated by Lennard-Jones atomic packing interactions, hydrogen bonding, and an implicit solvation model, as previously described (14). In the second stage of design, we enumerated all combinations of amino acid changes frequently observed as stabilizing in design round one and ranked the resulting structures relative to wild-type (see Table 1 and "Experimental Procedures"). Accordingly, the second-stage "design space" was biased toward low-scoring sequences predicted to be more stable than wild type, but also contained some residue combinations predicted to be less stable than wild type (Fig. 1*C*). We constructed 25 MICA variants by site-directed mutagenesis to test variants with design scores both better and worse than wild type. Mutants are named by the positions at which they differ from wild type as MICmutant_mutant. All mutants were expressed in *Escherichia coli* as inclusion bodies, refolded by stepwise dialysis, and purified by nickel-affinity chromatography followed by preparative SEC.

Characterization of Mutant MICA—Mutants were well behaved in several assays. All MICA mutants and wild type with the exception of MICQ120I_K154M eluted from SEC columns in sharp, ~30-kDa peaks; CD spectra of MICA mutants (Fig. 2*A*) taken from 200 to 250 nm at 25 °C were similar to wild type; and intrinsic tryptophan fluorescence spectra for mutants were coincident with the wild-type MICA spectrum (data not shown). The loss of ellipticity with increased temperature associated with unfolding was observed by CD at T_m = 47.5 °C for wild type. Ten representative mutants showed 50% loss of ellipticity at temperatures ranging from 33.0 °C for MICK152E_K154M to 54.6 °C for MICN69Q_D72F_Q108L_K152V_Y157L, or higher for MICN69Q_Q108L_Q120I_K154S_T155D, which did not exhibit an upper-baseline loss of signal even at 95 °C (Fig. 2*A*). Except for K152E_K154M, the nine mutants retained full ellipticity at physiological temperature.

The transition measured by CD and the local stability of the α2 helix region are distinct phenomena that may not be related. The local secondary structure predicted to be influenced by the eight designed mutations consists of two α-helical turns and a loop. This is a fraction of the total secondary structure in MICA and is not necessarily part of the overall structural transition observed by CD. Six mutant T_m values are similar to wild type, melting within a 5° range. Of the four mutants with T_m values >5° from wild-type, the two predicted to be destabilized have lower T_m values, and the two predicted to be stabilized have higher T_m values.

Some MICA mutants were predicted to be destabilized by tryptophans introduced at buried positions (N69W and D72W), which we probed with fluorescence quenching. Acrylamide quenches solvent-contacting tryptophan side chains but is too polar to penetrate into a folded protein (19). When titrated with acrylamide up to 300 mM, MICN69W_K152E and MICN69W_D72W_ K152E fluorescence at 350 nm decreased linearly, despite the buried nature of residues 69 and 72 (Fig. 2*B*). Acrylamide quenching of wild-type tryptophan fluorescence plateaued by 150 mM, so some tryptophan residues in wild type appear too buried for the acrylamide to contact. The predicted destabilization did not result in a loss of global thermal stability for the mutant with the greatest predicted destabilization, MICN69W_K152E (Fig. 2*A*), or loss of solution monodispersivity measured by SEC for any protein other than MICQ108I_K154M. Because these mutants maintain global

structure according to SEC and CD, any structural disruption resulting in solvent exposure of the introduced tryptophans appears local.

Equilibrium SPR Affinity of Mutant MICA for NKG2D—Mutant binding to NKG2D was assessed at equilibrium by SPR. Mutant MICA molecules and wild-type MICA were amine-coupled to sensor chips. NKG2D injections resulted in increased signal and a flat response corresponding to binding equilibrium within 60–75 s (Fig. 3, *A* and *B*). Plots of equilibrium response *versus* [NKG2D] gave affinities in terms of dissociation constants, $K_{D\,eq}$, in the nanomolar to low micromolar range. Contrary to our original hypothesis, none of the 15 MICA mutants predicted to stabilize the receptor-bound conformation exhibited significantly increased affinity for NKG2D (defined as $\Delta\Delta G_{eq} < -0.4$ kcal mol^{-1}, where $\Delta\Delta G_{eq} = \Delta G_{mutant\,eq} - \Delta G_{WT\,eq}$ and $\Delta G_{eq} = RT \ln K_{D\,eq}$) (Table 2). However, 10 MICA mutants were predicted to *destabilize* the receptor-bound conformation, and five of these bound to NKG2D with $\Delta\Delta G_{eq} \leq -0.9$ kcal mol^{-1} (Table 3). We confirmed these findings in solution with 1:1 molar injections of all MICA mutants and NKG2D through an analytical SEC column (20), after which the five destabilized/enhanced-affinity MICA mutants eluted as bound complexes with NKG2D at ~60 kDa, whereas wild-type and stabilized mutants did not (data not shown).

Monophasic Mutant MICA-NKG2D Kinetics Observed by SPR—The kinetics of mutant binding to NKG2D could also be assessed by SPR. The SPR response changes before reaching equilibrium could be fit with a monophasic 1:1 Langmuir binding model for wild-type and all MICA mutants predicted to stabilize the wild-type conformation (Fig. 3, *C* and *D*; see "Experimental Procedures" for fitting details). $K_{D\,kin\,obs}$ was calculated from $k_{off\,obs}/k_{on\,obs}$, which was converted to ΔG and compared with wild-type affinity using $\Delta\Delta G$ (Table 2). $\Delta\Delta G_{kin}$, defined as $\Delta G_{mutant\,kin} - \Delta G_{WT\,kin}$, correlates with $\Delta\Delta G$ from equilibrium fits (Fig. 3*G*), showing that the observed kinetics recapitulate the relative equilibrium results, as with TEM1-BLIP mutants (21).

Within this set of mutants (Table 2), $k_{on\,obs}$ did not change by >2-fold relative to wild type (for one mutant, $k_{on\,obs}$ decreased by a factor of 2.5). $k_{off\,obs}$ also did not change by >2-fold (15 mutants) (Fig. 3*H*). From $\Delta\Delta G_{kin}$, seven mutants bind NKG2D with unchanged affinities within error relative to wild-type, three bind better, and three bind worse, but none deviate by >0.4 kcal mol^{-1}. Therefore, the mutations predicted to stabilize the receptor-bound MICA conformation changed kinetic parameters by <2-fold and did not significantly alter affinity for NKG2D.

SPR response data were collected from 10 to 37 °C and subjected to linear van't Hoff thermodynamic analysis (Fig. 4*A*). Wild-type MICA is both entropically and enthalpically driven, as previously reported (10), regardless of kinetic model (Tables 2 and 3). The van't Hoff enthalpies for this set of MICA mutants interacting with NKG2D are all higher than wild type (Fig. 5*A*), showing that entropy has become more of a driving force for the set. Because the free energies of interaction are either similar or weaker, the enthalpic component becomes less of a driving force as the entropic component becomes more of one.

TABLE 3
MICA mutants predicted to destabilize the receptor-bound conformation and fit with a biphasic kinetic model

All thermodynamic values are given at 25 °C in kcal mol^{-1}. Des. score rel. to WT = mutant design score − wild-type design score (see Table 2). ΔG_{bi}, ΔG_1, ΔG_2, and related van't Hoff enthalpies were calculated from $K_{A1} = k_{+1}/k_{-1}$, $K_{A2} = k_{+2}/k_{-2}$, and $K_{Abi} = (k_{+1}/k_{-1}) + (1 + k_{+2}/k_{-2})$ (22). For MICD72W, affinities were too weak at temperatures other than 25 °C for reliable multiphasic fitting, and the enthalpy is derived from monophasic fits as from Table 2.

MIC mutant	Design score rel. to WT	ΔG_{eq}	$k_{+1}/10^3$	$k_{-1}/10^{-3}$	$k_{+2}/10^{-3}$	$k_{-2}/10^{-3}$	ΔG_{bi}	ΔH_{VH}	ΔG_1	ΔH_1	ΔG_2	ΔH_2
			$M^{-1}\,s^{-1}$	s^{-1}	$M^{-1}\,s^{-1}$	s^{-1}						
Wild-type	0	−7.3 ± 0.1	14.4 ± 0.6	74 ± 5	16.2 ± 1.3	13.6 ± 0.8	−7.7 ± 0.1	−4.1 ± 0.6	−7.2 ± 0.6	−2.2 ± 0.6	−0.10 ± 0.01	−3.0 ± 0.7
D72W	0.3	−6.9 ± 0.1	18.8 ± 1.6	174 ± 18	13.5 ± 1.9	30.8 ± 3.2	−7.1 ± 0.1	−0.6 ± 3.1	−6.9 ± 0.9	N/A	0.63 ± 0.16	N/A
Q120I	0.7	−8.2 ± 0.1	45.3 ± 1.9	67 ± 5	20.3 ± 1.7	9.4 ± 0.8	−8.6 ± 0.1	−9.3 ± 2.2	−8.0 ± 0.7	−6.3 ± 1.8	−0.36 ± 0.04	−3.7 ± 1.8
Q120I_K154M	0.8	−7.5 ± 0.3	27.4 ± 1.6	143 ± 8	15.7 ± 0.8	12.7 ± 0.6	−7.7 ± 0.1	3.4 ± 1.4	−7.2 ± 0.6	3.8 ± 1.4	−0.13 ± 0.01	−1.0 ± 0.4
N69W	1.8	−8.2 ± 0.1	50.0 ± 0.6	46 ± 1	15.0 ± 0.3	11.3 ± 0.1	−8.8 ± 0.1	−3.5 ± 0.7	−8.2 ± 0.2	5.4 ± 0.9	−0.16 ± 0.01	−15.3 ± 0.8
N69W_K152E_K154S	4.2	−8.8 ± 0.1	245.0 ± 8.0	118 ± 6	34.8 ± 1.6	16.3 ± 0.2	−9.3 ± 0.1	−7.7 ± 1.0	−8.6 ± 0.5	−0.2 ± 1.7	−0.43 ± 0.02	−11.6 ± 1.1
N69W_K152E_K154D	4.3	−8.8 ± 0.1	170.0 ± 2.0	58 ± 2	23.5 ± 0.7	10.1 ± 0.1	−9.5 ± 0.1	−8.5 ± 0.9	−8.8 ± 0.3	−5.6 ± 1.0	−0.49 ± 0.02	−5.5 ± 2.6
K152E_K154M	4.4	−7.4 ± 0.2	22.7 ± 1.0	91 ± 5	9.1 ± 0.5	9.5 ± 0.7	−7.8 ± 0.1	3.4 ± 1.5	−7.4 ± 0.5	3.0 ± 1.3	0.02 ± 0.01	0.4 ± 0.9
N69W_D72F_K152E	4.5	−7.3 ± 0.1	43.5 ± 1.3	171 ± 5	10.1 ± 0.6	20.5 ± 0.8	−7.8 ± 0.1	0.1 ± 2.8	−7.4 ± 0.3	2.0 ± 2.3	0.16 ± 0.02	−6.2 ± 3.4
N69W_D72W_K152E	5.1	−7.2 ± 0.2	49.8 ± 1.5	205 ± 5	7.3 ± 0.4	24.1 ± 1.1	−7.5 ± 0.1	−10.4 ± 3.1	−7.4 ± 0.3	−1.9 ± 1.3	0.64 ± 0.05	−15.8 ± 3.2
N69W_K152E	5.5	−8.4 ± 0.1	80.3 ± 0.9	35 ± 1	11.7 ± 0.3	10.0 ± 0.1	−9.1 ± 0.1	−6.7 ± 0.8	−8.7 ± 0.2	−1.8 ± 0.8	−0.08 ± 0.01	−8.9 ± 1.0

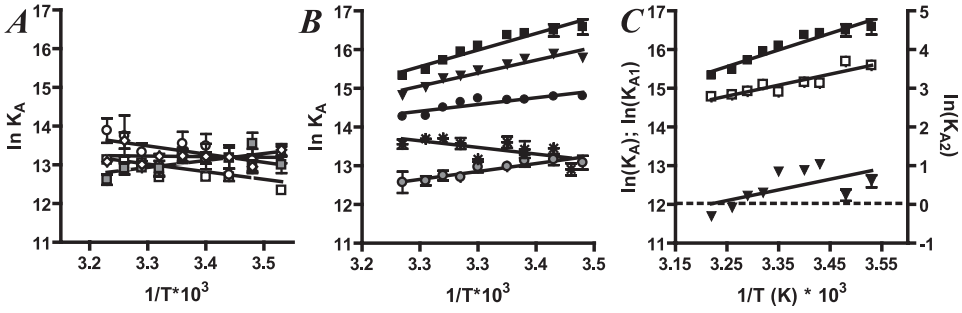

FIGURE 4. **Van't Hoff analysis of SPR data.** *A*, van't Hoff plots of wild type and three representative mutants predicted to stabilize receptor-bound structure, fit as monophasic kinetics. Slopes of fit lines tilt relative to wild type to indicate entropy-driven thermodynamic changes. MICA WT = *gray squares*; MICK154D = *white circles*; MICN69Q_K154D = *white triangles*; MIC N69Q_D72F_Q108L = *white diamonds*. *B*, van't Hoff plots of wild type and four representative mutants predicted to destabilize receptor-bound structure, fit as biphasic kinetics. MICA WT = *gray circles*; MICK152E_K154M = *asterisks*; MICN69W = *circles*; MICN69W_K154E = *triangles*; MICN69W_K152E_K154D = *squares*. *C*, van't Hoff plots of overall affinity constant and constants for individual steps for MICN69W_K152E_K154D, as described in Table 3. Overall = *squares*; step 1 = *white squares*; step 2 = *triangles*.

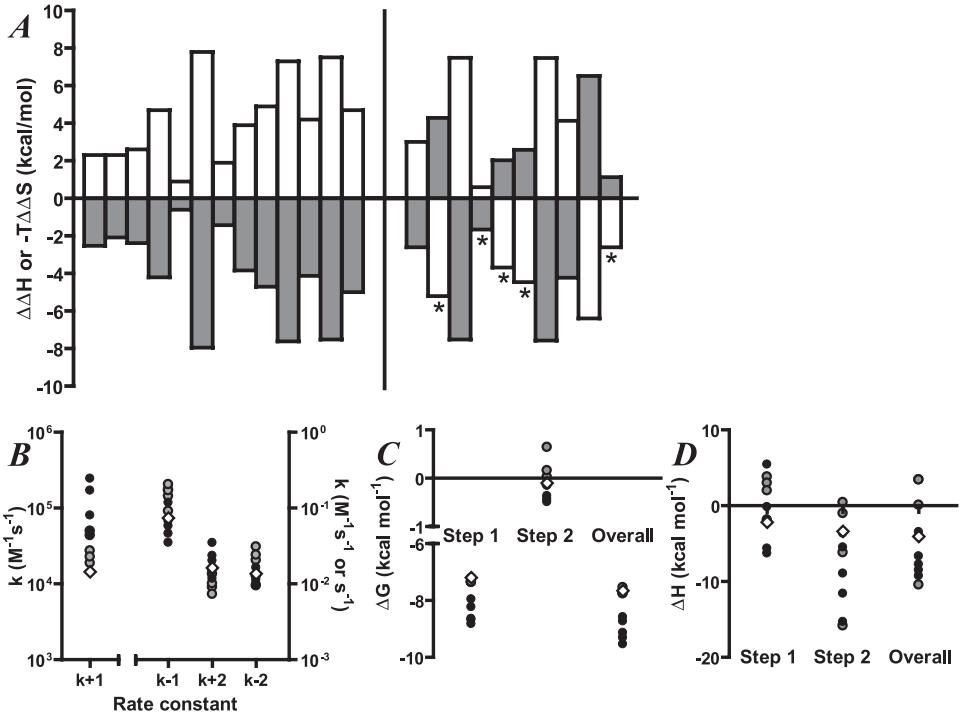

FIGURE 5. **Entropy and enthalpy changes upon mutation and biphasic rate constants observed by SPR.** *A*, changes in enthalpy and entropy for MICA mutants binding NKG2D arranged by predicted stabilization of the receptor-bound MICA conformation. Mutants are arranged according to design scores, with lowest scores (predicting most stabilized receptor-bound MICA conformation) on the *left* and highest score (predicting most destabilized receptor-bound conformation) on the *right*, and the *vertical bar* in the middle representing wild-type MICA-NKG2D. Thermodynamics are shown relative to wild type, as $\Delta\Delta H = \Delta H$ mutant $- \Delta H$ wild type = *white bars*, and $-T\Delta\Delta S = -T\Delta S$ mutant $-(-T\Delta S$ wild type) = *gray bars*. The five affinity-enhanced MICA mutants are highlighted with *asterisks*, four of which are enthalpy-stabilized and one of which does not change from the enthalpy-driven thermodynamic signature of wild type. *B*, the four biphasic rate constants for the 10 mutants predicted to be destabilized from the receptor-bound conformation. *C*, free energies of binding for the two steps from biphasic fits. *D*, enthalpies of binding for the two steps from biphasic fits. For *B–D*, wild type = *white diamond*; four destabilized mutants with similar affinities to wild type = *gray circles*; five destabilized mutants with enhanced affinities = *black circles*.

Biphasic Mutant MICA-NKG2D Kinetics Observed by SPR—For the mutants predicted to destabilize the receptor-bound MICA conformation, two kinetic phases can be observed during both NKG2D association and dissociation, which are best fit by a two-step binding model (Fig. 3, *E* and *F*). For comparison, MICA wild type can be fit with a two-step mechanism, giving kinetic and thermodynamic results similar to those from poor monophasic fits and equilibrium results, but most of the stabilized MICA mutants bind NKG2D too weakly for both phases to be observed by SPR. Several control tests found no evidence of weak nonspecific binding, sample inhomogeneity, or coupling artifacts (see "Experimental Procedures"). $\Delta\Delta G_{bi}$ $(= \Delta G_{mutant\ bi} - \Delta G_{WT\ bi})$ calculated from the four kinetic constants of the two-step fit correlates with $\Delta\Delta G_{eq}$ (Fig. 3*G*). When monophasic fits were used for destabilized mutants, we found similar affinities and rate constants, but poorer fits with larger residuals.

In a two-step model, a fast "encounter" step precedes a slower "docking" step (22, 23). If destabilized MICA mutants have lost local structure and become more induced-fit in mechanism, a slower docking step could result. The amplitude of the second dissociation phase increased when injection time was increased, k_{+1} was concentration-dependent, and k_{+2} was concentration-independent, consistent with two-step induced-fit binding.

Of the 10 destabilized MICA mutants, all exhibit increased k_{+1}, by up to 17-fold for MICN69W_K152E_K154S, a mutant predicted to be moderately destabilized from the receptor-bound conformation. The dissociation phases, k_{-1} and k_{-2}, and the second association phase, k_{+2}, vary no more than 3-fold from wild type, respectively. The intermediate constants, k_{+2} and k_{-1}, showed some variation with mutation relative to wild type, but only k_{+1} showed a significant, constant change for all destabilized mutants (Fig. 5*B*). Five destabilized mutants have dissociation rates similar to wild type and therefore bind NKG2D with affinities enhanced by 0.9–1.8 kcal mol^{-1} (Fig. 3*H*). Four mutants bind identically within error, and MICD72W binds more weakly, because faster association coincides with faster dissociation.

The four SPR-observed rate constants have different responses to temperatures from 10 °C to 37 °C, which were fit to lines in van't Hoff plots as separate steps (Fig. 4, *B* and *C*) (24). MICN69W_K152E, the mutant with the highest predicted destabilization, a high affinity for NKG2D, and strong

enthalpic stabilization of interaction, was cross-checked for affinity and enthalpy by ITC, which confirmed van't Hoff results (ITC $\Delta G = -9.3 \pm 0.1$ at 31 °C and SPR $\Delta G_{bi} = -9.1 \pm 0.1$ kcal mol^{-1} at 30 °C; ITC $\Delta H = -7.35 \pm 0.11$ and SPR $\Delta H_{VH} = -6.7 \pm 0.8$ kcal mol^{-1}). For the 10 proteins amenable to biphasic van't Hoff analysis, the encounter step provides most of the free energy of interaction and is entropy-driven (Fig. 5, compare *C* and *D*). The docking step is close to equilibrium and is enthalpy-driven. These thermodynamic signatures were also observed for two-step induced-fit antibody-antigen interactions: cases where molecules can approach quickly, driven by long range electrostatics, but must wait for flexible surfaces to shift before forming specific, enthalpy-driven contacts in the final complex (23).

DISCUSSION

MICA binding has been enhanced 0.9–1.8 kcal/mol, or ~15-fold in terms of K_D, by 1–3 mutations at residues that do not contact receptor in the wild-type complex structure. This gain in binding energy is similar to that attained by other rational redesigns of direct protein-protein contacts (12, 13). We aimed to decrease the entropic cost of binding by non-covalently stabilizing a disordered, flexible helix/loop structure that becomes ordered upon binding. These mutations primarily affected association phase kinetics, as expected, and produced the expected changes in entropy of interaction, but the direction of their effect on affinity was opposite to that of the original hypothesis. All mutants with affinity enhanced by >1 kcal mol^{-1} and association rate enhanced by 3-fold or more are enthalpy-driven and have design scores worse than wild type. The highest-affinity mutants are MICN69W_K152E_K154D and MICN69W_ K152E_K154S, which are predicted to be moderately destabilized from the wild type receptor-bound conformation.

The set of association-enhancing mutations contains a number of different types of substitutions alone and in combination. Each is predicted to destabilize the receptor-bound MICA conformation and can potentially perturb the binding surface. The bulky D72W, D72F, and K154M substitutions accelerated k_{+1} but also accelerated either k_{-2} or k_{-1} (Table 3) and so may alter contacts important to complex stabilization. The bulky N69W and smaller Q120I, K152E, K154S, and K154D substitutions accelerated k_{+1} without large changes in the other three constants. Long range electrostatic interactions drive initial encounter (25–27), and many of these substitutions involve adding or removing a charge, but point mutants Q120I and N69W accelerate k_{+1} by >3-fold and ΔG by 0.9 kcal mol^{-1} or more without changing an ionizable side chain.

We observed two kinds of compensations in this set of mutants: kinetic and thermodynamic. Kinetically, our enhanced-affinity mutants showed a slow, secondary k_{+2} association phase, but a faster initial k_{+1}. The same structural alteration that causes the slower phase may also enhance the faster phase, producing observable biphasic kinetics. Thermodynamically, the phenomenon of entropy-enthalpy compensation has been observed in a variety of protein-ligand interactions (28, 29). In this case, decreasing the entropic cost of protein-protein association resulted in an overcompensatory enthalpic penalty. Conversely, in four out of five cases, enhanced affinity is accompanied by an enthalpic stabilization that overcompensates for the predicted entropic destabilization. If, as the crystallographic evidence suggests, a folding event either precedes or accompanies binding, the second, enthalpy-driven step of the observed biphasic association may represent a helix-folding event. The enthalpy of α helix folding has been estimated at ~−1 kcal mol^{-1} per residue (30). In an interesting structural parallel to MICA-NKG2D, hydrogen-deuterium exchange study of a human growth hormone variant-receptor interaction revealed that enhanced affinity is caused by a disordered binding-site α helix that becomes more ordered upon binding (31).

How could "destabilizing" mutations accelerate association? We do not know what kind of local structural or dynamic alterations result from these mutations, beyond our observation that global structure is largely maintained. Possibilities include local loss of structure, unintentional enhancement of electrostatics, stabilization of a new backbone conformation that promotes binding, and/or removal of a structural feature that hinders binding. Of these, the first is a general mechanism consistent with the diversity of substitution types and locations resulting in accelerated kinetics, the observation of entropic destabilization coupled with affinity enhancement, the fact that a moderate predicted destabilization had the strongest effect on affinity, and the increased acrylamide quenching of tryptophan mutants. Disorder could increase association through a combination of a "fly-casting" mechanism (32), a local ground-state destabilization (31), and/or a post-"encounter" phase enhancement of a "search" phase at the expense of "docking" kinetics (33).

Structural definition of the dynamics of 10 residues of putative local disorder in a set of ~30-kDa mutant proteins is not trivial. We will further characterize these MICA mutants to understand the mechanism of association enhancement. Also, now that triple mutants of MICA have been produced with significantly increased NKG2D association rates, we can next attempt to rationally design decreased dissociation rates by optimizing MICA-NKG2D contacts.

Acknowledgments—We thank Ian Horner, Michael Jones, Collin Hauskins, Tyson Chung, Andrew VanSchoiack, Daniel Rowe, Jennifer Olson, Chad Mayer, Patrick Nygren, Kalani Snyder, and Seattle Pacific University BIO/CHM4362 winter quarter students for their excellent technical assistance. We are grateful to Colin Current for his help in CD experiments.

REFERENCES

1. Bauer, S., Groh, V., Wu, J., Steinle, A., Phillips, J. H., Lanier, L. L., and Spies, T. (1999) *Science* **285,** 727–729
2. Groh, V., Steinle, A., Bauer, S., and Spies, T. (1998) *Science* **279,** 1737–1740
3. Groh, V., Bahram, S., Bauer, S., Herman, A., Beauchamp, M., and Spies, T. (1996) *Proc. Natl. Acad. Sci. U. S. A.* **93,** 12445–12450
4. Li, P., Willie, S. T., Bauer, S., Morris, D. L., Spies, T., and Strong, R. K. (1999) *Immunity* **10,** 577–584
5. Li, P., Morris, D. L., Willcox, B. E., Steinle, A., Spies, T., and Strong, R. K. (2001) *Nat. Immunol.* **2,** 443–451
6. Dyson, H. J., and Wright, P. E. (2002) *Curr. Opin. Struct. Biol.* **12,** 54–60
7. Natarajan, K., Hicks, A., Mans, J., Robinson, H., Guan, R., Mariuzza, R. A., and Margulies, D. H. (2006) *J. Mol. Biol.* **358,** 157–171

8. Holmes, M. A., Li, P., Petersdorf, E. W., and Strong, R. K. (2002) *J. Immunol.* **169,** 1395–1400
9. Adams, E. J., Chien, Y. H., and Garcia, K. C. (2005) *Science* **308,** 227–231
10. McFarland, B. J., and Strong, R. K. (2003) *Immunity* **19,** 803–812
11. McFarland, B. J., Kortemme, T., Yu, S. F., Baker, D., and Strong, R. K. (2003) *Structure* **11,** 411–422
12. Song, G., Lazar, G. A., Kortemme, T., Shimaoka, M., Desjarlais, J. R., Baker, D., and Springer, T. A. (2006) *J. Biol. Chem.* **281,** 5042–5049
13. Clark, L. A., Boriack-Sjodin, P. A., Eldredge, J., Fitch, C., Friedman, B., Hanf, K. J., Jarpe, M., Liparoto, S. F., Li, Y., Lugovskoy, A., Miller, S., Rushe, M., Sherman, W., Simon, K., and Van Vlijmen, H. (2006) *Protein Sci.* **15,** 949–960
14. Kortemme, T., Morozov, A. V., and Baker, D. (2003) *J. Mol. Biol.* **326,** 1239–1259
15. Miley, M. J., Messaoudi, I., Metzner, B. M., Wu, Y., Nikolich-Zugich, J., and Fremont, D. H. (2004) *J. Exp. Med.* **200,** 1445–1454
16. Dantas, G., Kuhlman, B., Callender, D., Wong, M., and Baker, D. (2003) *J. Mol. Biol.* **332,** 449–460
17. Calhoun, D. B., Vanderkooi, J. M., and Englander, S. W. (1983) *Biochemistry* **22,** 1533–1539
18. Li, Y., Lipschultz, C. A., Mohan, S., and Smith-Gill, S. J. (2001) *Biochemistry* **40,** 2011–2022
19. Calhoun, D. B., Vanderkooi, J. M., Holtom, G. R., and Englander, S. W. (1986) *Proteins* **1,** 109–115
20. Steinle, A., Li, P., Morris, D. L., Groh, V., Lanier, L. L., Strong, R. K., and Spies, T. (2001) *Immunogenetics* **53,** 279–287
21. Reichmann, D., Cohen, M., Abramovich, R., Dym, O., Lim, D., Strynadka, N. C., and Schreiber, G. (2007) *J. Mol. Biol.* **365,** 663–679
22. Lipschultz, C. A., Li, Y., and Smith-Gill, S. (2000) *Methods* **20,** 310–318
23. Lipschultz, C. A., Yee, A., Mohan, S., Li, Y., and Smith-Gill, S. J. (2002) *J. Mol. Recognit.* **15,** 44–52
24. Li, Y., Urrutia, M., Smith-Gill, S. J., and Mariuzza, R. A. (2003) *Biochemistry* **42,** 11–22
25. Selzer, T., Albeck, S., and Schreiber, G. (2000) *Nat. Struct. Biol.* **7,** 537–541
26. Kiel, C., Selzer, T., Shaul, Y., Schreiber, G., and Herrmann, C. (2004) *Proc. Natl. Acad. Sci. U. S. A.* **101,** 9223–9228
27. Schreiber, G. (2002) *Curr. Opin. Struct. Biol.* **12,** 41–47
28. Keeble, A. H., Kirkpatrick, N., Shimizu, S., and Kleanthous, C. (2006) *Biochemistry* **45,** 3243–3254
29. Krishnamurthy, V. M., Bohall, B. R., Semetey, V., and Whitesides, G. M. (2006) *J. Am. Chem. Soc.* **128,** 5802–5812
30. Avbelj, F., Luo, P., and Baldwin, R. L. (2000) *Proc. Natl. Acad. Sci. U. S. A.* **97,** 10786–10791
31. Horn, J. R., Kraybill, B., Petro, E. J., Coales, S. J., Morrow, J. A., Hamuro, Y., and Kossiakoff, A. A. (2006) *Biochemistry* **45,** 8488–8498
32. Shoemaker, B. A., Portman, J. J., and Wolynes, P. G. (2000) *Proc. Natl. Acad. Sci. U. S. A.* **97,** 8868–8873
33. Selzer, T., and Schreiber, G. (2001) *Proteins* **45,** 190–198